Published in the Proceedings of the 16th International Aluminum Alloys Conference (ICAA16) 2018
ISBN: 978-1-926872-41-4
by the Canadian Institute of Mining, Metallurgy & Petroleum

MECHANICAL PROPERTIES OF PRECIPITATION HARDENED SUPERSATURATED Al-Sc-Zr

*Yang Yang, Joseph Licavoli, and Paul Sanders

Michigan Technological University
Houghton, Michigan, USA
*(*Corresponding author: yyang10@mtu.edu)*

ABSTRACT

Al-Sc-Zr alloys form thermally stable $L1_2$ precipitates which provide high temperature strength. Although the overall fraction of $L1_2$ Al_3Sc and Al_3Zr may be increased by increasing scandium (Sc) and zirconium (Zr) content, such additions may increase primary phase fractions and do not produce desirable secondary phase morphologies. Rapid solidification techniques, such as melt spinning, increase solute atom concentration within the matrix. When the supersaturated matrix is aged, higher precipitate volume fractions at low Sc and Zr levels can be achieved improving high temperature strength. Melt spinning was used to rapidly solidify (10^7 k/s) a thin ribbon of Al-0.5Sc-0.4Zr at. %. The ribbon was compacted and extruded into 99.8% dense rods, and then aged using multi-step isochronal heat treatment up to 600°C. Precipitation strengthening was evaluated by ambient hardness measurement. The ambient hardness of melt-spun ribbon after precipitation hardening increased by 450 MPa (~67% increment) during isochronal heat treatment.

KEYWORDS

Aluminum alloys, Precipitation strengthening, Scandium, Zirconium, Rapid solidification, Extrusion

INTRODUCTION

Small Sc and Zr additions to aluminum improve strength and creep resistance above 300°C due to tri-aluminide precipitation of $Al_3(Sc, Zr)$ in $L1_2$ structures similar to γ' $Ni_3(Al, Ti)$ in nickel superalloy, but the $Al_3(Sc, Zr)$ particles have a Sc-rich core surrounded by Zr-rich shell (Figure 1). The Al_3Zr shell limits atomic transport between the Al_3Sc core and the matrix and reduces coherency strain. These factors reduce precipitate coarsening rate at elevated temperature (Bergner & Van Chi, 1977; Fujikawa, 1997; Knipling et al., 2011; Clouet et al., 2006).

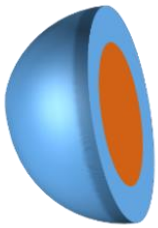

Figure 1. Simplified schematic model of precipitate Al(Sc,Zr) in Al-Sc-Zr alloy. Shell is rich of Al(Zr) intermetallic phase, particle core is rich of Al(Sc) intermetallic phase (after Voorhees, 2006).

Numerous $Al_3(Sc, Zr)$ particles increase alloy strength and creep resistance as the precipitates impede dislocation glide and to a lesser extent climb. Previous work on ternary Al-Sc-Zr alloys show large strength increases versus binary Al-Sc, and Al-Zr alloys in Table 1.

Table 1. Maximum Vickers hardness of Al-0.06Sc, Al-0.06Zr, and Al-0.06Sc-0.06Zr at. % during isothermal heat treatment from room temperature to 600°C, 25°C per 3 h step (Knipling et al., 2011).

Alloy (at. %)	Heat treatment	Microhardness (MPa)	Increment (%)
Al-0.06Sc	To 325°C	415	48.2
Al-0.06Zr	To 500°C	295	180
Al-0.06Sc-0.06Zr	To 400°C	615	–

The Vickers microhardness of Al-0.06Sc-0.06Zr at. % alloy (at 400°C) is about 42% and 108% larger than Al-0.06Sc at. % and Al-0.06Zr at. %, respectively. This strength enhancement is explained by considering the Orowan mechanism, which is governed by:

$$\Delta\sigma_{or} = M \cdot \frac{0.4 \cdot G_{Al} \cdot b}{\pi\sqrt{1-v}} \cdot \frac{\ln\left(\frac{2\bar{R}}{b}\right)}{\lambda_{e-e}} \quad (1)$$

where M is the Taylor mean orientation factor, b is the matrix Burgers vector of aluminum, v is the precipitate volume fraction, $\bar{R}$ is the mean precipitate radius size, and G_{Al} is the matrix shear modulus (Meyers & Chawla, 1983), and $\lambda_{e-e} = \bar{R}\left(\sqrt{\frac{2\pi}{3f}} - \frac{\pi}{2}\right)$ is the edge-to-edge inter-precipitate spacing (Courtney, 2005). The Al_3Zr shell limits Al_3Sc coarsening at elevated temperature. As a result, the average precipitate radius in Al-Sc-Zr alloys is about four times smaller than binary Al-Sc alloys with congruent composition (8.8 nm vs. 2.3 nm after aged at 300°C for 72 h) (Fuller et al., 2003; Marquis & Seidman, 2001). According to Equation 1, smaller precipitate size at similar volume fraction decreases precipitate spacing and more readily restricts dislocation motion via the Orowan mechanism.

Ternary Al-Sc-Zr precipitate strengthening is limited by low solubility of Sc and Zr in the matrix. Table 2 shows equilibrium solid solubility (C_{400} for binary Al-X alloys), and diffusivities of Sc, Zr and some common aluminum alloy additions at 400°C (Barabash, Sulgenko, Legkaya, & Korzhova, 2001;

Bergner & Van Chi, 1977; Feufel, Gödecke, Leo Lukas, & Sommer, 1997; Fujikawa, Hirano, & Fukushima, 2016; Fujikawa, 1997).

Table 2. Equilibrium maximum solid solubility (C_{400} for binary Al-X alloys) and diffusivities of Sc, Zr and some common aluminum alloy additions at 400°C. Diffusion distance is calculated based on diffusivities at 400°C for one second.

Element	C_{400} (at. %)	D_{400} m^2/s	$d = \sqrt{Dt}$ (m), t=1s
Sc	0.01	2.0×10^{-17}	4.47×10^{-9}
Zr	0.0005	1.2×10^{-20}	1.09×10^{-10}
Cu	0.74	1.5×10^{-15}	3.87×10^{-8}
Si	1.05	3.5×10^{-13}	5.91×10^{-7}

The solubilities of Sc and Zr are at least two magnitudes smaller than common aluminum alloying additions such as Cu and Si. When Sc and Zr additions exceed solution saturation level in conventional casting, they will form undesirable primary second phase particles. Primary precipitates not only effect alloy strength, but also act as nucleation sites during aging creating inhomogeneity.

Precipitation volume fraction may be increased via melt spinning to produce supersaturated alloys. Melt spinning involves ejecting a thin molten metal stream onto rotating copper wheel. The molten metal simultaneously solidifies on and is propelled forward by the wheel forming thin ribbon (~50 um thick in this experiment). A supersaturated solid solution is formed as atomic motion is limited during rapid solidification. Table 3 summarizes the effects of cooling rate on solute concentration in Al-X binary alloys (Sc and Zr).

Table 3. The composition of rapidly solidified Al-X alloys (Toropova et al., 1998)

Cooling rate, K/s	Concentration at given cooling rate (at. %)	
	Sc	Zr
10^1	0.4	0.1
10^3	1.1	0.5–0.7
10^5	3.2	1.2–2.0
10^7	–	3.78

In melt spinning, the cooling rate of the ejected metal decreased significantly with distance from the rotating copper wheel. This implies that with rapid solidification, inhomogeneity is still possible in the side of the ribbon opposite the wheel surface. The Aziz-Kaplan continuous growth models (CGM) (Aziz, 1982) describe how the velocity v of the interface and partition coefficient k change with temperature difference as:

$$v = \frac{v_c(T_i)}{RT_i}(-\Delta G_{eff}) \tag{2}$$

$$k = \frac{k_e + (v/v_D)}{1 + \left(\frac{v}{v_D}\right) - (1 - k_e)X_L} \tag{3}$$

where $v_c(T_i)$ is a kinetic coefficient, T_i is the interface temperature, ΔG_{eff} is a molar Gibbs free energy change of solidification, $k_e$is the equilibrium partitioning parameter, v_D is the diffusive coefficient, and X_L is the molar fraction of liquid phase. Values of v and k decrease due to the cooling rate decreases away from contact side, resulting in reduced solute-trapping from contact to non-contact side of the wheel.

The ambient temperature strengthening of supersaturated Al-Sc-Zr alloys is examined in the current work. Concentrations of Sc and Zr were increased until primary phases appeared. An Al-0.5Sc-0.4Zr at. % alloy was chosen based on alloy screening trials. Ribbon solidification rates were determined by secondary dendrite arm spacing (SDAS) measurements (S. Haselhuhn, Sanders, & Pearce, 2017). Isochronal heat treatment was employed on melt-spun ribbon and on extruded consolidated rods to promote finely dispersed $Al_3(Sc, Zr)$ precipitates within the matrix. Mechanical properties were estimated by ambient temperature hardness tests.

EXPERIMENTAL PROCEDURES

Experimental Flow and Design

The concentrations of Sc and Zr were increased incrementally to 0.8 at. % and analyzed with X-ray diffraction (XRD) to determine solubility limit in melt-spun ribbon. The maximum solubility of Sc or Zr in solution was determined at the concentration where the lattice parameter of the Al-matrix no longer increased with increasing solute addition. Sc and Zr additions up to 0.8 and 0.55 at. %, respectively were confirmed in the previous works (Deane, Kampe, Swenson, & Sanders, 2017). This is much less than Toropova's (1998) binary result of Al-3.78at%Zr and Al-3.7at%Sc with 10^7K/s cooling rate. A nominal sample composition of Al-0.5Sc-0.4Zr at. % was chosen given the negative solubility interaction between Sc and Zr.

The experimental flow is shown in Figure 2. A supersaturated Al-0.5Sc-0.4Zr at. % ternary alloy was produced through melt spinning, consolidation and extrusion. After melt spinning, primary precipitate formation and actual composition were evaluated using environmental scanning electron microscopy (ESEM) and inductively coupled plasma optical emission spectroscopy (ICP-OES). Consolidation and extrusion were performed after no primary precipitation was observed in melt-spun ribbon. Low concentration of Al-0.06Sc-0.06Zt at. % was vacuum induction melting (VIM) casted using tensile bar candelabra mold.

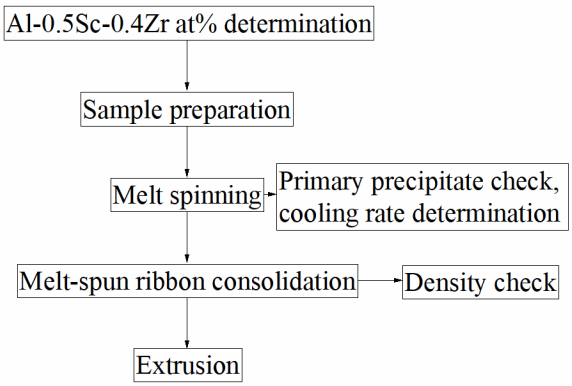

Figure 2. Flow chart of experiment design to produce supersaturated Al-Sc-Zr extruded consolidation melt-spun ribbon.

Alloy Preparation

Several ~15 g charges consisting of 99.99% pure Al, Al-2Sc wt. % and Al-10Zr wt. % master alloys were prepared for melt spinning. The master alloys were sliced into small pieces to fit in the crucible. All materials were cleaned using ethanol and ultrasonic bath to remove contamination.

Melt Spinning

Quartz crucibles with ~0.7 mm orifices were prepared for melt spinning. The interior of each crucible was coated with aluminum oxide spray to prevent silicon contamination at high temperatures ($3SiO_2 + 4Al \rightarrow 2Al_2O_3 + 3Si$). The melt spinner chamber was evacuated to 8×10^{-5} torr and backfilled to 400 torr with 99.99% pure argon. The backfill line was reopened when materials melted preventing from backpressure buildup and dripping. The charge was heated to 1100°C and held 1 min holding times using optical observation and a Micro-Epsilon ratio pyrometer (0.5% accuracy, 5 ms response time). The melt was then ejected onto a rotating copper wheel (~1800 RPM) and deposited into a collection tube.

Rate of Solidification Determination

Melt-spun ribbon cross sections were mounted and finish polished using 0.04-micron colloidal silica. Average second dendrite arm spacing (SDAS) were measured using 500X optical microscopy. Solidification rate was estimated by correlating SDAS measurements to solidification rates found in previous work (Haselhuhn, Sanders, & Pearce, 2017).

Ribbon Consolidation

Precipitation was avoid by consolidating ribbon at room temperature. A 170-mm height compaction die was machined with 19.5 mm diameter tube (Figure 3). Ribbon was compacted into ~25 mm long and 19.5 mm Ø rod under 125 KN load (Carver press). The density of consolidated rod was estimated using Archimedes principle. Compared with as-cast rod, the consolidated rod was ~90% dense.

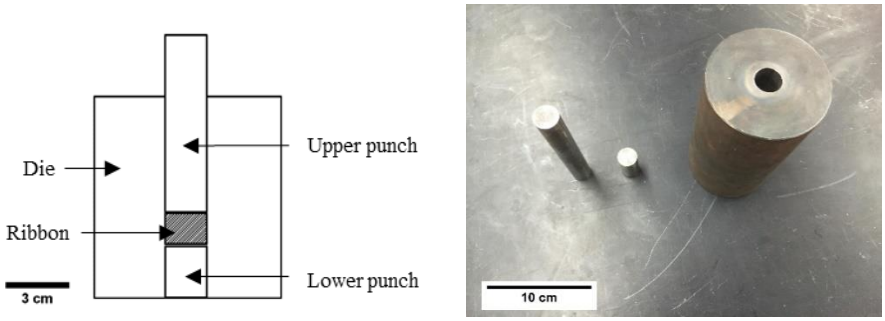

Figure 3. Simplified sectional drawing of compaction die. Melt-spun ribbon was chopped and inserted between two punches. Ribbon was compacted into ~25 mm long and 19.5 mm Ø rod with 125 KN load.

Extrusion

The extrusion die set is shown in Figure 4. A high reduction ratio of 15:1 was used for further consolidate. Despite potential early precipitation, it was necessary to preheat both the die and ribbon to decrease flow stresses. The extrusion die was pre-heated to 300°C using cartridge heaters and the consolidated rod was underwent a 10 min pre-heat to ~200°C. The exit speed of the extruded rod was approximatly 5 cm/min with a final diameter of 4.5 mm. The extruded rod was air cooled and stored at room temperature. The low concentration of as-cast Al-0.06Sc-0.06Zt at. % rod underwent identical extrusion with same reduction ratio and extrusion rate.

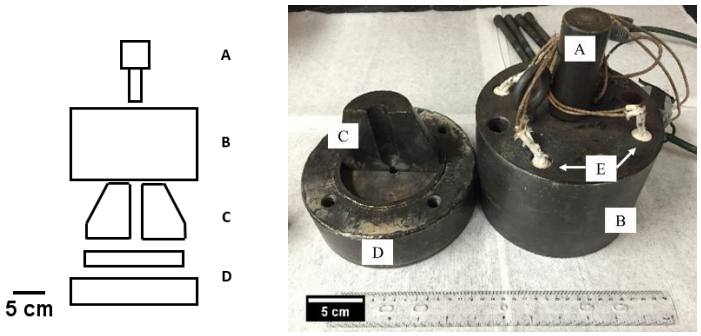

Figure 4. Simplified schematic extrusion hardware consists of ram (A), outer shell (B), extrusion die (C), bottom plate (D), and four cartridge heaters are inserted in outer shell (E).

Heat Treatments, Microhardness

Isochronal heat treatments were applied to melt-spun ribbon and extruded rods from room temperature to 600°C in 25°C increments for 3 hours per increment. After each treatment step, the sample was water quenched, polished, and microhardness was measured. Precipitation hardening changes were measured by Vickers or Knoop microhardness depending on samples size and shape. A Vickers indenter was used for bulk samples and Knoop indenter was used for thin melt-spun ribbon. Both Vickers and Knoop hardness tests used 50 g loads and 15 s dwell times with 10 measurements per sample (using IS unit MPa=HV/HK×9.807). Hardness measurement results of Vickers and Knoop vary with different loads, the hardness trendlines reflected hardness change consistently (George, 2012; Yovanovich, 2006).

RESULTS AND DISCUSSION

Melt-Spun Ribbon Microstructure

The melt-spun ribbon was consistently ~5 mm wide and ~50 μm thick. As cooling rate decreased from the copper-contact side (left) to non-contact side (right), primary precipitates are observed concentrated near in the non-contact side as shown in Figure 5a.

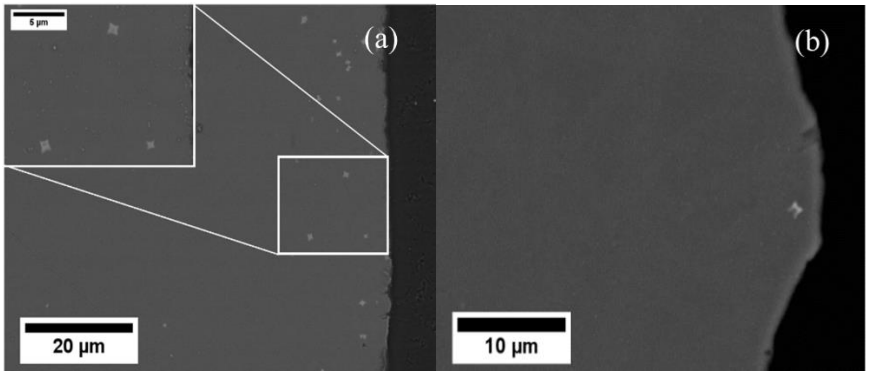

Figure 5. ESEM micrograph of mechanical polished Al-0.5Sc-0.4Zr at. % melt-spun ribbon underwent different ejection pressures. Petal-shape primary precipitates are observed on the non-contact surface side in (a). Number of primary precipitate is much smaller in (b) using decreased ejection pressure from 0.15 psi to 0.13 psi.

Several modifications to wheel rotation rate (1500–1800 RPM) and melt expulsion pressure (0.15–0.13 psi), resulted in finer ribbon with few primary precipitates (Figure 5b).

Solidification Rate

The determination of an accurate cooling rate is significant because it impacts solubility limits. An etched ribbon sample is shown in Figure 6, where fine dendrites are observed due to Zr and Sc microsegregation.

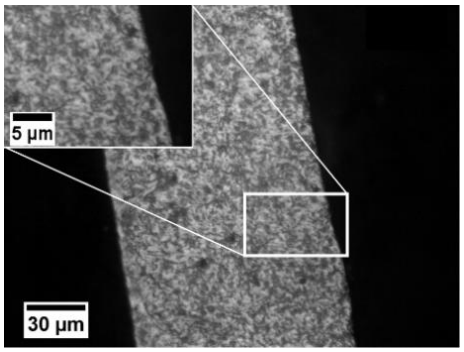

Figure 6. Melt-spun Al-0.11Sc-0.5Zr at. % ribbon cross-section, etched with Barker's reagent, optical microscopy 500X.

The cooling rate is calculated from:

$$\text{Cooling Rate} = \left(\frac{\text{SDAS}}{\text{B}}\right)^{-1/\text{n}} \tag{4}$$

where B and n are fitting factors for aluminum alloy (Haselhuhn et al., 2017). SDAS is determined from average measurement values. The cooling rate provided using melt spinning is 1.1×10^7 K/s at 1500 rpm. The primary precipitate concentration near non-contact side implies a composition differential across ribbon. ESEM line scans on the aluminum matrix through ribbon section (Figure 5a) revealed solute change shown in Figure 7.

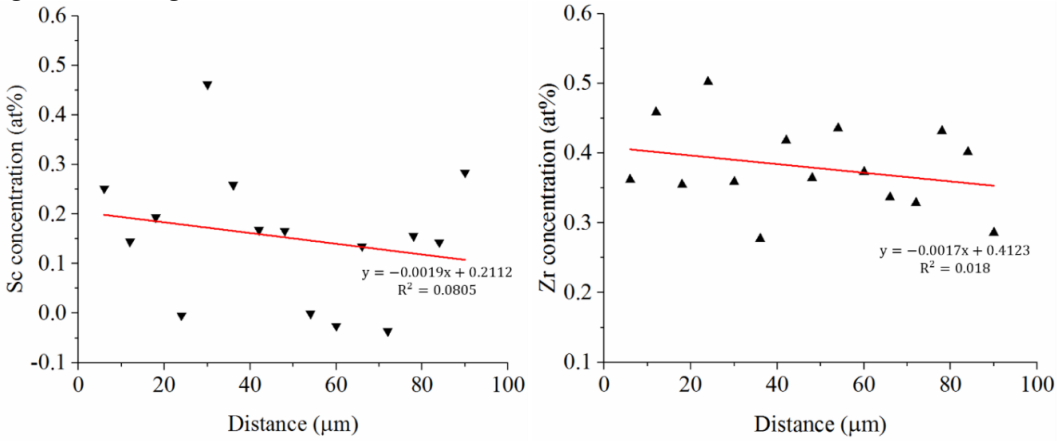

Figure 7. Concentrations of Sc and Zr decrease through melt-spun ribbon cross section from contact side (left) to non-contact side (right) using ESEM line scan on ribbon cross section shown in Figure 5a.

Two linear fitting lines indicate that both concentrations gradient of Sc and Zr is ~–0.002 at%/µm from left to right. These trendlines generally confirm the effects of primary precipitation on matrix composition, which influence precipitation evolution and properties measured after isochronal heat treatments.

Ambient Temperature Hardness

Hardness tests on unsaturated ternary Al-0.06Sc-0.06Zr at. % alloy are shown in Figure 8. Four different processing routes were used to produce samples which underwent identical isochronal heat treatment. These processing routes include as-cast, extruded as-cast, melt-spun ribbon, and consolidated/extruded rod.

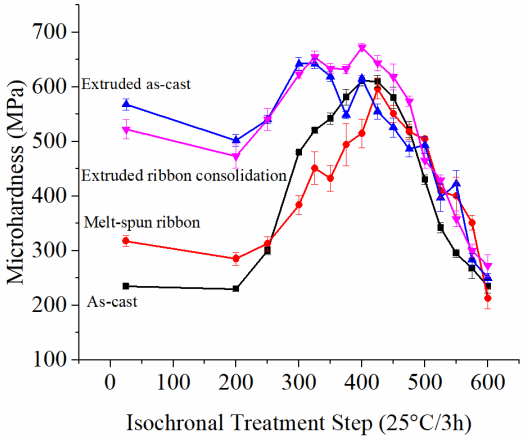

Figure 8. Isochronal heat treatments on Al-0.06Sc-0.06Zr at. %: as-cast rod, extruded as-cast rod, melt-spun ribbon, and consolidated/extruded rod. The range of heat treatment from room temperature to 600°C, 25°C per step lasting 3 hours. Microhardness of melt-spun ribbon is Knoop hardness, other three are measured using Vickers hardness (all with 50 g load and 15 s dwell; using IS unit MPa=HV/HK×9.807).

The extruded as-cast and consolidated/extruded ribbon rod (Vickers), have over 200 MPa higher hardness than as-cast (Vickers) and melt-spun ribbon (Knoop) at room temperature. Moreover, this hardness difference remains until peak hardness is achieved at 325°C. The hardness gaps narrow at 400°C except for extruded consolidation ribbon rod which increased. All samples lose strength at the same rate after 400°C.

Extrusion demonstrated the highest contribution to alloy strength, over 200 MPa higher from room temperature to 300°C. It increased alloy hardness until sample has been heat treated to 425°C. Since concentrations of Sc and Zr are within the solubility limit for Al-0.06Sc-0.06Zr at. % alloy, melt spinning does not provide any additional Sc or Zr into solution, meaning volume fraction of precipitation should be and was unchanged.

Melt spinning's contribution is only apparent when the alloy is supersaturated. The hardness of Al-0.5Sc-0.4Zr at. % melt-spun ribbon that underwent identical isochronal heat treatment as above is shown in Figure 9.

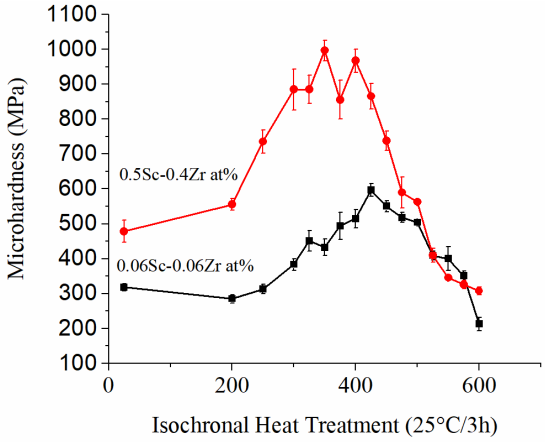

Figure 9. Hardness change after isochronal heat treatment on Al-0.06Sc-0.06Zr at. %melt-spun ribbon vs Al-0.5Sc-0.4Zr at. % melt-spun ribbon. The range of heat treatment from room temperature to 600°C, 25°C per step for 3 h. All results are Knoop hardness with 50 g load and 15 s dwell; using IS unit MPa=HV/HK×9.807.

With almost ten times the solute concentration in the aluminum matrix, the hardness of Al-0.5Sc-0.4Zr at. % melt-spun ribbon is 90% higher than low concentration ribbon. The hardness of melt-spun Al-0.5Sc-0.4Zr at. % is at least 200 MPa larger than low concentration alloys from room temperature to 400°C, and the hardness difference reaches 450 MPa at 425°C. With reference to Equation 1, the solute concentrations was increased in supersaturated melt-spun ribbon and assuming the precipitate size is constant, the hardness increment can be attributed to the higher precipitate volume fraction.

CONCLUSIONS

In this study, melt spinning was used to increase solute concentration. Concentrations of Sc and Zr were increased to Al-0.5Sc-0.4Zr at. % without significant primary precipitation. The supersaturation of Sc and Zr decreased from wheel contact side to non-contact side due to the lower cooling rate. The cooling rate was estimated at 1.1×10^7 K/s at 1500 RPM from SDAS calculations. Ribbon consolidation and extrusion enabled bulk testing of this supersaturated alloy. Extruded as-cast and consolidation Al-0.06Sc-0.06Zr at. % have over 200 MPa higher than non-extruded samples (as-cast and melt-spun) from room temperature to 300°C in isochronal heat treatment (Figure 8). Isochronal heat treatment of melt-spun Al-0.06Sc-0.06Zr at. % and melt-spun Al-0.5Sc-0.4Zr at. % with subsequent room temperature microhardness indicate contributions from increased volume fraction of precipitates. Compared with melt-spun Al-0.06Sc-0.06Zr at. %, melt-spun Al-0.5Sc-0.4Zr at. % has a peak hardness which is 450 MPa higher at 425°C (Figure 9). Future work will focus on volume fraction of precipitate change with increased amount of Sc and Zr, the precipitate size change as a function of supersaturation, and how extrusion changes grain size and precipitate morphology.

ACKNOWLEDGMENTS

We would like to thank Paul Fraley, Thomas Wood, and Russell Stein for experimentation assistance and helpful discussions; and the Office of Naval Research for sponsoring this work (N000141612878).

REFERENCES

Abed, E. J. (2014). Rapidly solidified of hyper eutectic aluminum-silicon alloys ribbons by using melt-spinning techniques. *International Journal of Current Engineering and Technology*, 4, 1394–1398.

Alshmri, F. (2012). Rapid Solidification Processing: Melt Spinning of Al-High Si Alloys. *Advanced Materials Research*, 383–390, 1740–1746. https://doi.org/10.4028/www.scientific.net/AMR.383—390.1740.

Aziz MJ. (1982). Model for solute redistribution during rapid solidification. *J. Appl. Phys*. 53:1158–1168. https://doi.org/10.1063/1.329867

Barabash, O. M., Sulgenko, O. V., Legkaya, T. N., & Korzhova, N. P. (2001). Experimental analysis and thermodynamic calculation of the structural regularities in the fusion diagram of the system of alloys Al-Mg-Si. *Journal of Phase Equilibria*, 22(1), 5–11. https://doi.org/10.1007/s11669-001-0049-3.

Bergner, D., & Van Chi, N. (1977). Untersuchungen zur Diffusion von 3 d-Metallen in Al [Investigations on the diffusion of 3 d metals in Al]. *Wissenschaftliche Zeitschrift Der Padagogischen Hochschule [Scientific Journal of The Padagogic College]*, 25, 15.

Clouet, E., Laé, L., Épicier, T., Lefebvre, W., Nastar, M., & Deschamps, A. (2006). Complex precipitation pathways in multicomponent alloys. Nature Materials, 5(6), 482–488. https://doi.org/10.1038/nmat1652.

Courtney, T. (2005). *Mechanical Beha vior of Materials* (2nd ed). Boston, MA: Waveland Pr Inc.

Deane, K., Kampe, S. L., Swenson, D., & Sanders, P. G. (2017). Precipitate Evolution and Strengthening in Supersaturated Rapidly Solidified Al-Sc-Zr Alloys. *Metallurgical and Materials Transactions A*, 48(4), 2030–2039. https://doi.org/10.1007/s11661-017-3982-4.

Feufel, H., Gödecke, T., Leo Lukas, H., & Sommer, F. (1997). Investigation of the Al-Mg-Si System by Experiments and Thermodynamic Calculations, *Journal of Alloys and Compounds*, 247, 31–42, https://doi.org/10.1016/S0925-8388(96)02655-2.

Fujikawa, S., Hirano, K., & Fukushima, Y. (2016). Diffusion of silicon in aluminum. *Metallurgical Transactions A*, 9(12), 1811–1815. https://doi.org/10.1007/BF02663412.

Fujikawa, S. I. (1997). Impurity Diffusion of Scandium in Aluminium. *Defect and Diffusion Forum*, 143–147, 115—120. https://doi.org/10.4028/www.scientific.net/DDF.143-147.115.

Fuller, C. B., Seidman, D. N., & Dunand, D. C. (2003). Mechanical properties of Al (Sc, Zr) alloys at ambient and elevated temperatures. *Acta Materialia*, 51(16), 4803–4814, https://doi.org/10.1016/S1359-6454(03)00320-3.

Fuller, C., & Seidman, D. (2005). Temporal evolution of the nanostructure of Al(Sc,Zr) alloys: Part II-coarsening of Al(ScZr) precipitates. *Acta Materialia*, 53, 5415–5428. https://doi.org/10.1016/j.actamat.2005.08.015.

George, V. (2012). Low-Load Vickers Microindentation Hardness Testing. *Advanced Materials and Processes*, 170(4), 28–33.

Haselhuhn, S. A., Sanders, P., & Pearce, J. (2017). Hypoeutectic Aluminum–Silicon Alloy Development for GMAW-Based 3-D Printing Using Wedge Castings. *International Journal of Metalcasting*, 11(4), 863–856. https://doi.org/10.1007/s40962-017-0133-z.

Knipling, K. E., Dunand, D. C., & Seidman, D. N. (2006). Criteria for developing castable, creep-resistant aluminum-based alloys–A review. *Zeitschrift Für Metallkunde [Journal of Metallurgy]*, 97(3), 246–265, https://doi.org/ 10.3139/146.101249.

Knipling, K. E., Karnesky, R. A., Lee, C. P., Dunand, D. C., & Seidman, D. N. (2010). Precipitation evolution in Al–0.1 Sc, Al–0.1 Zr and Al–0.1 Sc–0.1 Zr (at. %) alloys during isochronal aging. *Acta Materialia*, 58(15), 5184–5195, https://doi.org/10.1016/j.actamat.2010.05.054.

Knipling, K. E., Seidman, D. N., & Dunand, D. C. (2011). Ambient- and High- Temperature Mechanical Properties of Isochronally Aged Al-0.06Sc, Al-0.06 Zr, and Al-0.06Sc-0.06Zr Alloys (at. %). *Acta Materialia*, 59(3), 943–954. https://doi.org/10.1016/j.actamat.2010.10.017.

Marquis, E. A., & Seidman, D. N. (2001). Nanoscale structural evolution of Al3Sc precipitates in Al(Sc) alloys. *Acta Materialia*, 49(11), 1909–1919. https://doi.org/10.1016/S1359-6454(01)00116-1.

Meyers, M. A., & Chawla, K. K. (1983). Mechanical Metallurgy: Principles and Application (1st edition). Englewood Cliffs, N.J: Prentice-Hall, Inc.

Murray, J. L. (1998). The Al-Sc (aluminum-scandium) system. *Journal of Phase Equilibria*, 19(4), 380–384. https://doi.org/10.1361/105497198770342120.

Seidman, D. N., Marquis, E. A., & Dunand, D. C. (2002). Precipitation strengthening at ambient and elevated temperatures of heat-treatable Al(Sc) alloys. *Acta Materialia*, 50(16), 4021–4035. https://doi.org/10.1016/S1359-6454(02)00201-X.

Toropova, L. S. (1998). Advanced Aluminum Alloys Containing Scandium: Structure and Properties. Philadelphia, PA: Gordon & Breach Science Publishers Inc.

Toropova, L. S., Eskin, D. G., Kharakterova, M. L., & Dobatkina, T. V. (1998). Advanced Aluminum Alloys Conta. Amsterdam, The Netherlands: Routledge Inc.

Voorhees, P. W. (2006). Alloys: Scandium overtakes zirconium. *Nature Materials*, 5(6), 435. https://doi.org/10.1038/nmat1663.

Yovanovich, M. M. (2006). Micro and Macro Hardness Measurements, Correlations, and Contact Models. *44th AIAA Aerospace Sciences Meeting and Exhibit*. https://doi.org/10.2514/6.2006-979.